

EXHIBIT A

The Electrochemistry of Diamond

by

Matthew Neil Latto

*University of Bristol
School of Chemistry
Faculty of Science*

A dissertation submitted to the University of Bristol in accordance with the
requirements of the degree of
Doctor of Philosophy in the Faculty of Science

September 2001

CONTENTS

word count (chapters 1 - 9): 29,227
word count (all text): 38,805



Table of Contents

Title
Abstract
Acknowledgements
Author's Declaration
List of Figures
List of Tables
Units and Nomenclature

- 1 Introduction
 - 1.0 Outline
 - 1.1 The History of Diamond
 - 1.2 Allotropes of Carbon
 - 1.3 Properties of Diamond
 - 1.4 The Synthesis of Diamond
 - 1.5 Uses of Diamond
 - 1.5.1 Abrasives
 - 1.5.2 Thermal Management
 - 1.5.3 Electronic Devices
 - 1.5.4 Optical Windows
 - 1.6 The Electrochemistry of Boron Doped Diamond
 - 1.7 Summary
 - 1.8 Outline of the Thesis
- 2 Growth and Characterisation of the Diamond Films
 - 2.0 Outline
 - 2.1 The Choice of Growth Technique
 - 2.2 The Reaction Gases
 - 2.3 The Mass Flow Controllers
 - 2.4 Dilution of the Diborane Gas
 - 2.5 The Deposition Chamber
 - 2.6 The Substrate Heater
 - 2.7 The Filaments
 - 2.8 The Substrates
 - 2.9 Electrical Contacts to the films
 - 2.9.1 Indium/Gallium Eutectic
 - 2.9.2 Silver Loaded Epoxy Resin
 - 2.9.3 Three Layer Metalisation
 - 2.9.4 Titanium Contacts
 - 2.9.5 Summary
 - 2.10 Typical Growth Conditions
 - 2.11 Secondary Ion Mass Spectroscopy
 - 2.12 Scanning Electron Microscopy
 and Optical Microscopy
 - 2.13 Laser Raman Spectroscopy
 - 2.14 Summary
- 3 Electrical Contacts
 - 3.0 Outline
 - 3.1 Introduction

- 3.2 Fabrication of Three Layer Metal Contacts
- 3.3 Fabrication of Titanium Underlayer Contacts
- 3.4 Characteristics of Silver Epoxy Resin Contacts
- 3.5 Characteristics of Evaporated Gold Contacts
- 3.6 Characteristics of Three Layer Metal Contacts
- 3.7 Characteristics of Titanium Underlayer Contacts
- 3.8 Four Point Probe Measurements
- 3.9 Summary
- 4 Standard Electrochemical Theory
 - 4.0 Outline
 - 4.1 Metal Electrochemistry
 - 4.2 Normal p-type Semiconductor Electrochemistry
 - 4.3 Highly Doped Semiconductors
 - 4.4 Surface State Mediated Electrode Transfer
 - 4.4.1 Contributions to the Applied Potential
 - 4.4.2 Contributions of the Helmholtz Layer and the Space Charge Region
 - 4.4.3 Electrical Charge at the Surface of a Semiconductor Electrode
 - 4.4.4 The Butler-Volmer Equation
 - 4.4.5 Schottky Diode
 - 4.4.6 Model
 - 4.5 Steady State Current
 - 4.6 Summary
- 5 The Electrochemistry of Highly Doped Diamond Films
 - 5.0 Outline
 - 5.1 Experimental Set-up
 - 5.1.1 Electrolyte Solutions
 - 5.1.2 Electrochemical Cells
 - 5.1.3 Reference Electrodes
 - 5.1.4 Counter Electrodes
 - 5.1.5 Potentiostats
 - 5.1.6 Faraday Cages
 - 5.2 The Cyclic Voltammetry Technique
 - 5.2.1 Reversible Electrode Dynamics
 - 5.2.2 Irreversible Electrode Dynamics
 - 5.2.3 Quasi-Reversible Electrode Dynamics
 - 5.3 Cyclic Voltammetry in Dilute Nitric Acid
 - 5.4 Cyclic Voltammetry of 4-Aminophenol
 - 5.5 Cyclic Voltammetry of Potassium Ferrocyanide
 - 5.6 Cyclic Voltammetry of Ferrous Sulphate and Ferric Sulphate
 - 5.7 Mott-Schottky Plots
 - 5.8 AC Impedance
 - 5.8 Moderately Doped Films
 - 5.9 Summary
- 6 The Electrochemistry of Low Doped Diamond Films
 - 6.0 Outline
 - 6.1 Experimental Set-up
 - 6.2 Surface Termination

- 6.3 Cyclic Voltammetry of oxygen-terminated low-doped diamond
 - 6.3.1 Cyclic Voltammetry of Ferrous Sulphate and Ferric Sulphate
 - 6.3.2 Cyclic Voltammetry of Potassium Ferrocyanide and Potassium Ferricyanide
 - 6.3.3 Cyclic Voltammetry of Other Redox Couples
- 6.4 Cyclic Voltammetry of hydrogen-terminated low-doped diamond
- 6.5 Cyclic Voltammetry of low-doped diamond with indeterminate surface termination
 - 6.5.1 Cyclic Voltammetry of Ferrous Sulphate and Ferric Sulphate
 - 6.5.2 Cyclic Voltammetry of Potassium Ferrocyanide and Potassium Ferricyanide in an Aqueous Solution of Potassium Chloride
 - 6.5.3 Cyclic Voltammetry of Potassium Ferrocyanide and Potassium Ferricyanide in an Aqueous Solution of Potassium Hydroxide
- 6.6 Concentration Effects
- 6.7 Mott-Schottky Plots
- 6.8 Summary
- 7 Theoretical Model for the Electrochemistry of Boron Doped Diamond
 - 7.0 Outline
 - 7.1 Interpreting the Metallic Behaviour of Highly Doped Diamond
 - 7.2 Explanation of the Metallic Behaviour of Highly Doped Diamond
 - 7.2.1 Hydrogen Terminated Diamond
 - 7.2.2 Oxygen Terminated Diamond
 - 7.3 The relationship between current density and applied potential
 - 7.3.1 Special cases of the current density - applied potential relationship
 - 7.3.1.1 The case where $|j_H^0| \gg |j|$
 - 7.3.1.2 The case where $|j| \gg |j_H^0|$
 - 7.3.1.3 The case where $|j_{SC}^0| \gg |j|$ and $j \approx j_H^0$
 - 7.3.2 The current density - applied potential relationship at intermediate values
 - 7.4 AC Impedance and the Surface State Model
 - 7.5 Interpreting the Semiconductor Behaviour of Low Doped Diamond
 - 7.6 Summary
- 8 Intensity Modulated Photocurrent Spectroscopy
 - 8.0 Outline
 - 8.1 Intensity Modulated Photocurrent Spectroscopy (IMPS)
 - 8.2 Experimental Set-up
 - 8.3 Experimental Results
 - 8.4 Theory
 - 8.4.1 Effect of Constant Illumination on the Current Density
 - 8.4.2 Effect of Modulated Illumination on the Current Density
 - 8.5 Summary
- 9 Conclusions
 - 9.1 Background
 - 9.2 Growth and Characterisation
 - 9.3 Electrical Contacts
 - 9.4 Standard Electrochemical Theory
 - 9.5 Electrochemistry of Highly and Moderately Doped Diamond Films
 - 9.6 Electrochemistry of Low Doped Diamond Films
 - 9.7 Electrochemical Theory for Boron Doped Diamond Films
 - 9.8 Intensity Modulated Photocurrent Spectroscopy

9.9 Possible Future Work

A Appendix A: Levels of Impurities

- A.1 potassium chloride, KCl
- A.2 potassium hydroxide, KOH
- A.3 sodium chloride, NaCl
- A.4 ferrous sulphate heptahydrate, $\text{FeSO}_4 \cdot 7\text{H}_2\text{O}$
- A.5 ferric sulphate pentahydrate, $\text{Fe}(\text{SO}_4)_3 \cdot 5\text{H}_2\text{O}$
- A.6 ferric nitrate nonahydrate, $\text{Fe}(\text{NO}_3)_3 \cdot 9\text{H}_2\text{O}$

B Appendix B: Summary of Diamond Growth RunsC Appendix C: References

Chapter 4

Standard Electrochemical Theory

4.0 Outline

- This chapter outlines the standard electrochemical theory on which this study was based.
- A comparison is made between the behaviour of metal and semiconductor electrodes.
- An expression is derived relating the steady state current to the overpotential for surface state mediated charge transfer.

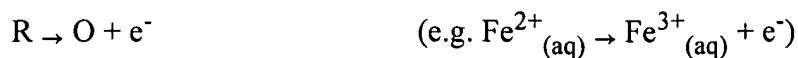
4.1 Metal Electrochemistry

In this section the Marcus-Gerischer theory for electron transfer at a metal electrode is outlined. Reference 119(a) contains details of the theory and lists the original references and review articles. Underlying this approach is the idea that electron transfer occurs between occupied and unoccupied states that are equal in energy.¹²⁰

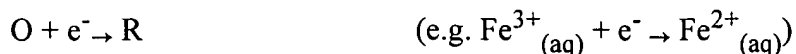
The total current density, j , at a metal-solution interface is the sum of the anodic current density, j_a , and the cathodic density, j_c . By convention, the cathodic current is negative.

$$j = j_a + j_c . \quad \text{(equation 4.1)}$$

Anodic current flows when oxidation occurs at the electrode surface:



Cathodic current flows when reduction occurs at the electrode surface:



In the Marcus-Gerischer approach to electron transfer it is assumed that the Born-Oppenheimer approximation applies, i.e., the nuclei, being so much heavier than the electron, move relatively slowly and may be treated as stationary during electron transfer.¹²¹ Hence electrons are transferred to energy levels at or near the Fermi level in the metal. At a metal electrode a change in the applied potential results in charging of the metal which leads to a change in the potential at the surface. As the energy of the surface electrons is altered the position of the Fermi level changes. However, the occupation of states about the Fermi level remains constant. As a result the current densities are simply proportional to the overlap integral of the Fermi function in the metal and the density of states function for the solution species:

$$j_a \propto (\text{overlap of } E_F \text{ and } E_R)$$

$$j_c \propto -(\text{overlap of } E_F \text{ and } E_O)$$

Figure 4.2 shows a schematic energy diagram for a metal-solution interface.

At the equilibrium potential, the overlap integrals are equal. The values of j_a and j_c are therefore equal and opposite and the net current density is zero. This situation is shown to the left in figure 4.2.

At a positive overpotential, the overlap integral for the reduced species is greater than that for the oxidised species. The net current density is therefore positive. An anodic current flows and oxidation of the reduced species occurs. This situation is shown in the upper right diagram in figure 4.2.

At a negative overpotential, the overlap integral for the oxidised species is greater than that for the reduced species. The net current density is therefore negative. A cathodic current flows and reduction of the oxidised species occurs. This situation is shown in the lower right diagram in figure 4.2.

Figure 4.1 shows a sketch of current density – overpotential relationship for the case where the transfer coefficient, $\alpha = \frac{1}{2}$.

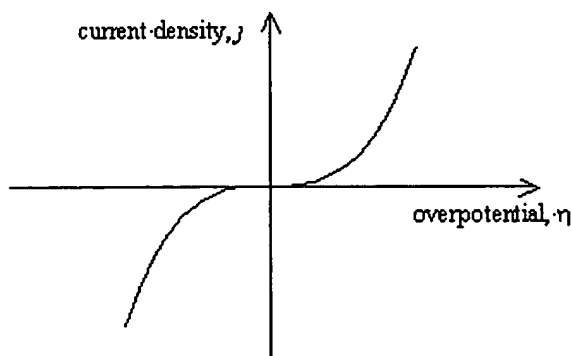


Figure 4.1 – current density as a function of overpotential for a metal

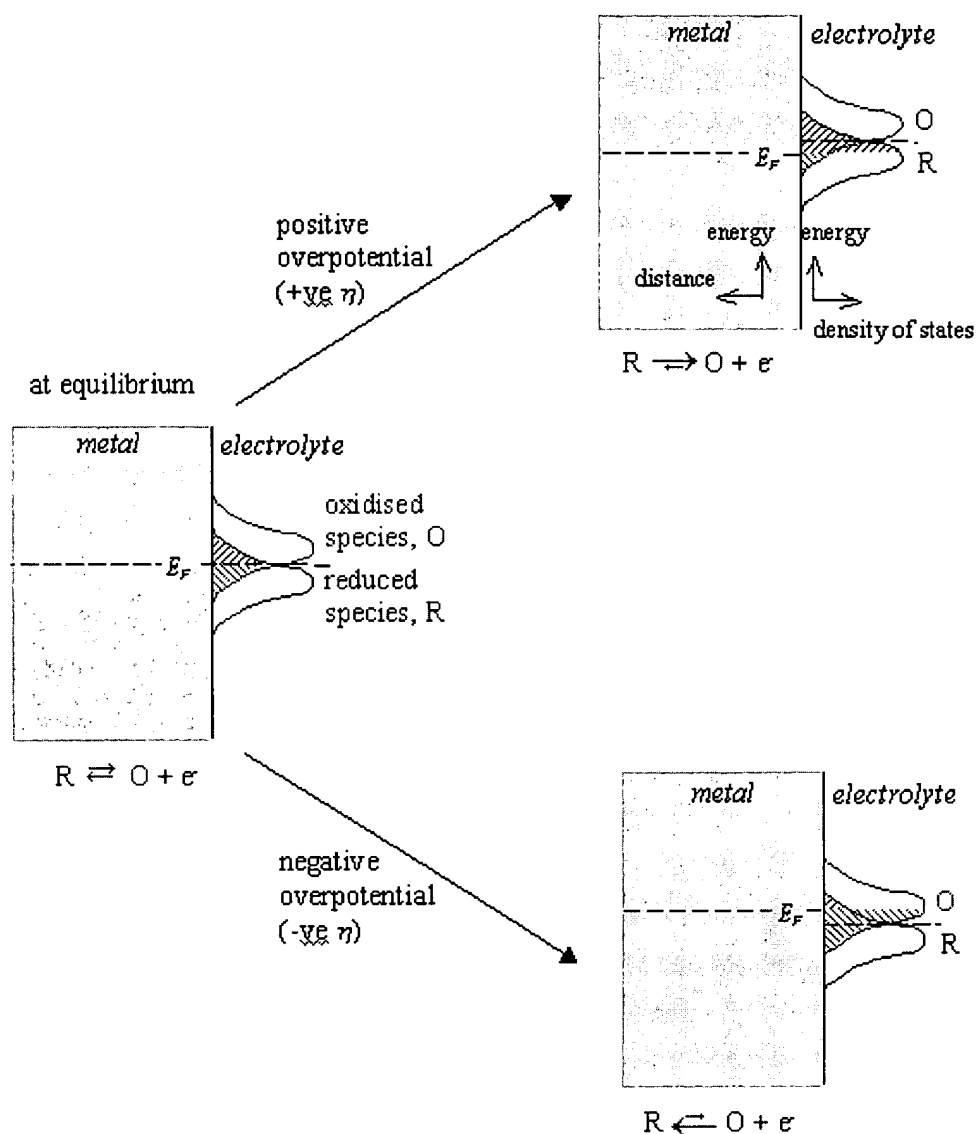
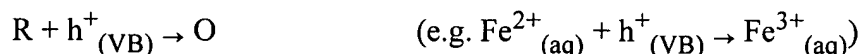


Figure 4.2 – Schematic Energy Diagram for a Metal-Solution Interface

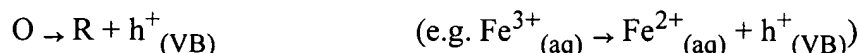
4.2 Normal p-type Semiconductor Electrochemistry

As for a metal electrode, the total current density, j , is the sum of the anodic and cathodic current densities (j_a & j_c). The majority charge carriers in a p-type semiconductor are positive holes in the valence band.

The anodic reaction:



The cathodic reaction:



The Born-Oppenheimer approximation still applies but unlike the case for a metal electrode, charge transfer can not occur at the Fermi level if the density of states is zero at that energy (i.e. it is in the band gap of the semiconductor). Charge transfer will occur at the surface energy of the valence band, $E_{VB,S}$.

Current flow at a semiconductor electrode is dependent of the surface concentration of majority charge carriers. For a p-type semiconductor, the concentration of holes at surface is a significant factor in the rate of charge flow in the anodic reaction:

$$j_a \propto (\text{overlap of } E_{VB,S} \text{ and } E_R) \times ([h^+]_{\text{surface}})$$

Whilst for the cathodic reaction the availability of electrons in the valence band is essentially constant:

$$j_c \propto - (\text{overlap of } E_{VB,S} \text{ and } E_O)$$

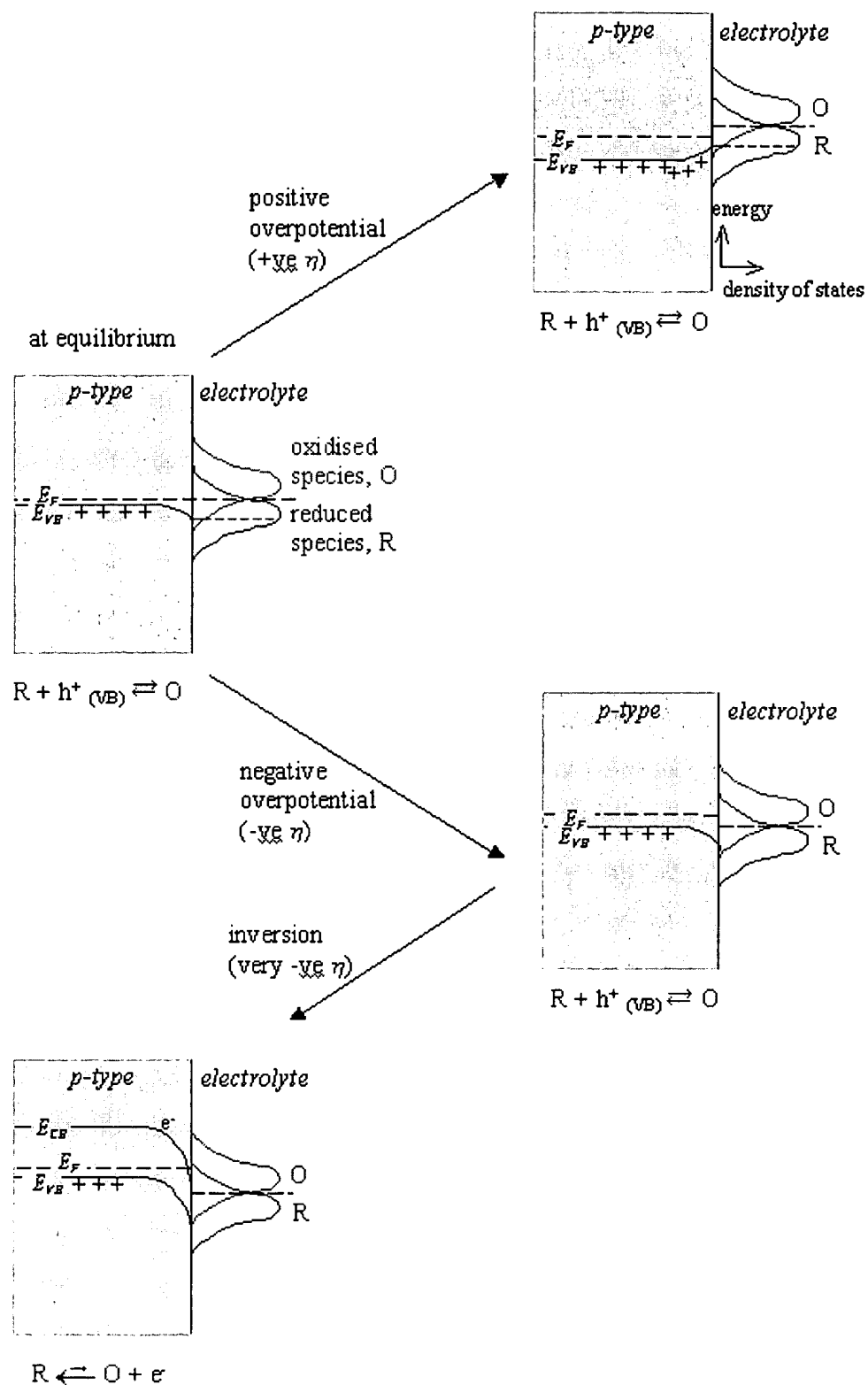


Figure 4.3 – Schematic Energy Diagram for a Semiconductor-Solution Interface

The overlap terms at the valence band edge are not affected by changes in potential. The cathodic current density will therefore remain constant.

$$j_c = j_{c,0}$$

At a positive overpotential, there will be a higher surface concentration of holes than at equilibrium. There is an exponential relationship between the concentration of holes and the overpotential. Therefore, at positive overpotential, the anodic current density will be greater than at equilibrium.

$$j_a > j_{a,0}$$

At negative overpotential, the concentration of holes at the surface will be reduced and as the magnitude of the negative overpotential is increased, the concentration will tend to zero. The anodic current density, j_a , will therefore fall from its equilibrium value, $j_{a,0}$.

The total current density, j , is the sum of the constant cathodic current density, j_c , and the variable anodic current density, j_a . At increasing positive overpotential, the total current density will rise rapidly, while at decreasing negative overpotential, the total current density will fall to a constant minimum value, equal to the equilibrium cathodic current density, $j_{c,0}$.

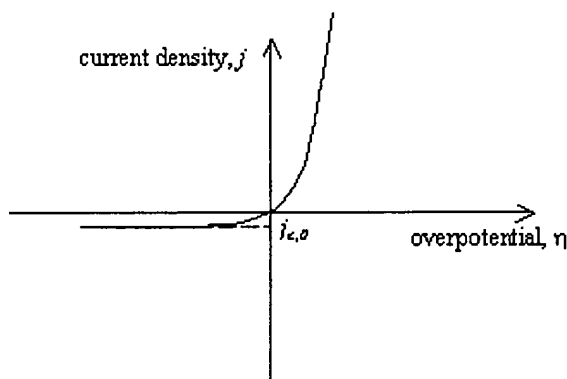
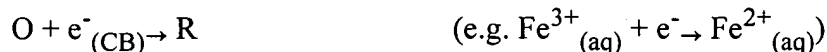


Figure 4.4 – current density as a function of overpotential for a semiconductor

At sufficiently negative potentials, inversion can occur. This phenomenon occurs when band bending at the surface of the semiconductor is sufficiently great that the Fermi level lies in the conduction band. There will then be a finite probability of finding a conduction band electron at the surface of the semiconductor. An anodic current can flow and the total current density will be reduced in magnitude ($j_{c,0} < j < 0$).

Anodic current flow due to inversion:



4.3 Highly doped semiconductors

At high doping levels, the semiconductor becomes *degenerately* doped. The Fermi Level of the semiconductor lies within the valence band (VB) and the space charge region becomes very small. Electrons are able to tunnel from the bulk VB directly into the electrolyte. Therefore, the concentration of available charge carriers is constant and the electrode behaves like a metal.

$$j_a \propto (\text{overlap of } E_F \text{ and } E_R)$$

$$j_c \propto - (\text{overlap of } E_F \text{ and } E_O)$$

Cyclic voltammograms will therefore show both oxidation and reduction peaks.

Figure 4.5 shows a schematic energy diagram for a highly doped semiconductor-solution interface.

Figure 4.6 shows a sketch of current density – overpotential relationship.

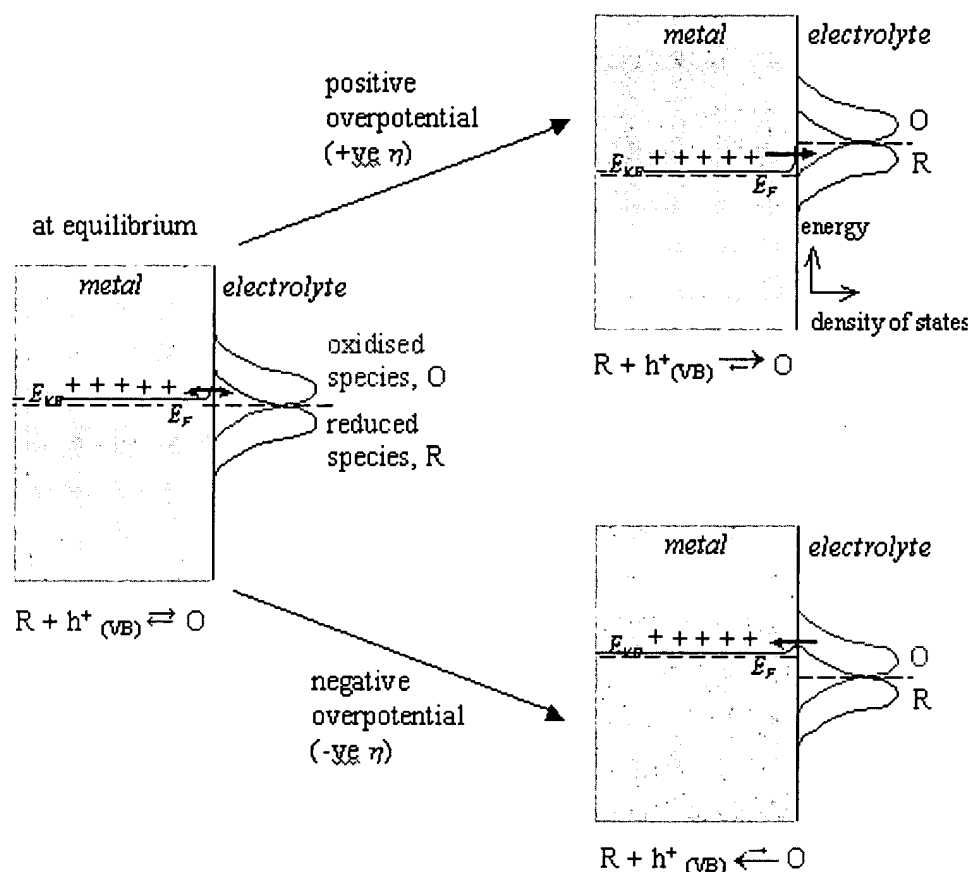


Figure 4.5 – Schematic Energy Diagram for a Heavily Doped Semiconductor-Solution Interface

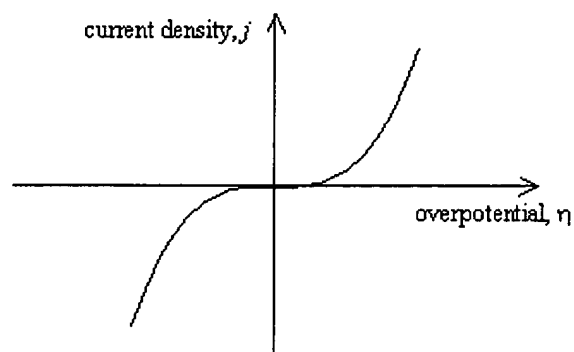


Figure 4.6 – current density as a function of overpotential for a heavily doped semiconductor